Article:
Al-Dhamri, HS, Abdul-Wahab, SA, Velis, C et al. (2020) Oil-Based Mud Cutting as an Additional Raw Material in Clinker Production. Journal of Hazardous Materials, 384. 121022. ISSN: 0304-3894

https://doi.org/10.1016/j.jhazmat.2019.121022

Oil-Based Mud Cutting as an Additional Raw Material in Clinker Production

Hilal S. Al-Dhamri[a,b,c], Sabah A. Abdul-Wahab[b], Costas Velis[c], Leon Black[c]*

[a] Oman Cement Company S.A.O.G, Muscat, Sultanate of Oman.
[b] Department of Mechanical and Industrial Engineering, Sultan Qaboos University, Muscat, Sultanate of Oman.
[c] School of Civil Engineering, University of Leeds, United Kingdom.

Abstract

Oil-Based Mud (OBM) cutting is a by-product generated during oil-well drilling. It is classified as a hazardous material; however, its chemical composition suggests that it might be suitable as a raw material in cement manufacturing. It is rich in calcium oxide, silica, and aluminium oxide, which are the major oxides in raw materials for cement manufacturing. In this research, OBM cutting is used as a constituent of the raw meal for cement clinker production. Raw meal mixtures were prepared by mixing different ratios of raw materials increasing OBM content. The impact of the addition of OBM cutting on the resulting clinker has been investigated. The results demonstrate that OBM cutting could be recycled in the manufacturing of Portland cement clinker. Clinker prepared using OBM cutting had very similar properties to that prepared from limestone. This result could represent an opportunity for solving an environmental problem.

The addition of OBM cutting lowers the calcination temperature, and increases the rate of carbonate dissociation. However, it also leads to a higher free lime content in the resulting clinker, which is a result of the presence of trace elements, such as barium. Overall, its use as a raw material in cement production could provide a cost-effective, environment-friendly route for the management of OBM cutting.

Graphical Abstract

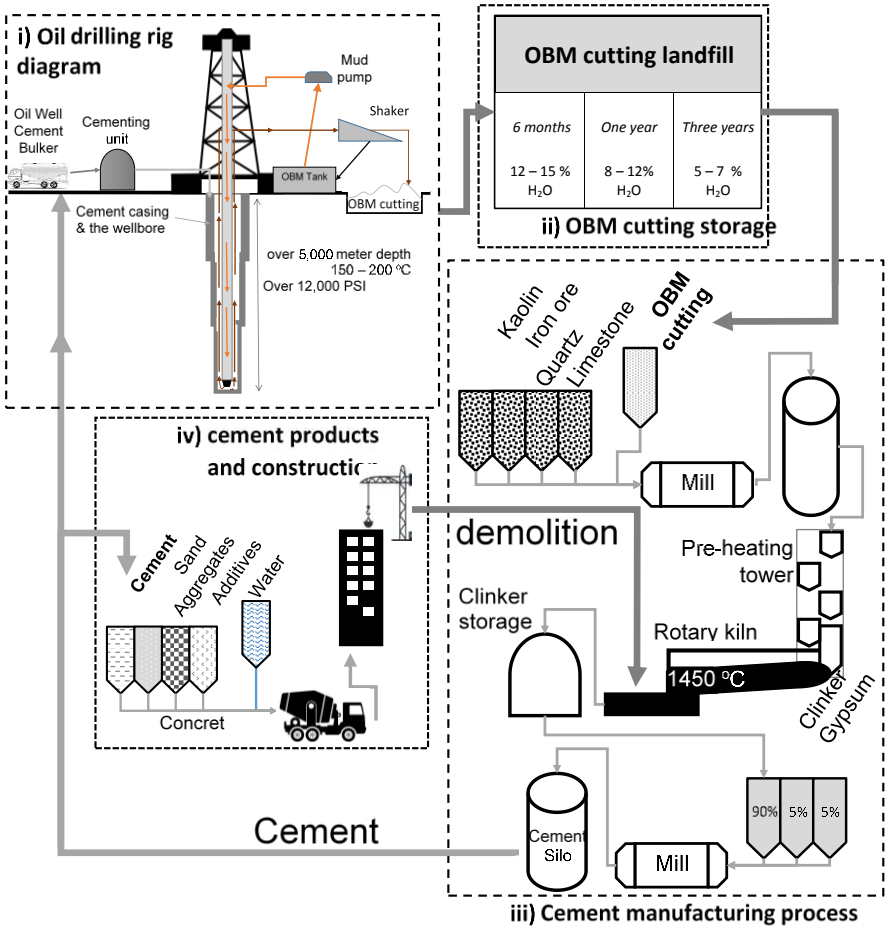

1 Introduction

There are several types of industrial hazardous by-products that are not yet utilised. Oil-Based Mud (OBM) cutting is an example of such materials [1–8]. OBM is produced during the oil-well drilling process. It contains oil, heavy metals, organic matter, and soil. During the drilling process of a single well, thousands of cubic metres of OBM cutting can be produced [9]. OBM cutting is classified as a hazardous material in Oman [10], with special storage specification enforced by the environmental authority [11].

OBM (also known as drilling fluid mud [1,2,12]), is the carrier of earth cutting during the drilling process and comes in many forms. The main role of the OBM is that of lifting the cutting up to the surface, thus permitting the drilling operation to move deeper [13–15]. Once the cuttings are collected at the surface, this mixture of drilling fluid and earth cuttings undergoes a segregation process for removing the cuttings and enabling the drilling fluid to be reused. This segregation step is repeated until the fluid can no longer be treated and is disposed of. The discarded fluid is known as Fluid-Based Mud cutting, the composition of which depends on the type of fluid used. Such type depends on the geological characteristics of the underground rocks. In many cases, Water-Based Mud [16] is used with the addition of some oil to improve some desirable properties of the drilling fluid and optimize the drilling process. This fluid is known as Oil-Based Fluid or Oil-Based Mud (OBM). The mud disposed from this process is known as Oil-Based Mud cutting (OBM cutting) and is collected in Mud Waste pits. OBM cuttings are contaminated with oil, which make them a potentially hazardous waste, and their release into the environment should be avoided.

OBM cuttings have several characteristics which could be exploited in the cement industry [17]. The cuttings contain calcium, silica, and alumina, which are essential components in cement manufacturing. Moreover, the oil content gives the cuttings a calorific value, which could help reduce the fuel demand during cement production. From the perspective of the oil industry, the use of cuttings in cement manufacturing would provide an environment-friendly waste management solution for a potentially hazardous waste. Such a solution is welcome because about 115,000 t of OBM cuttings are currently stored across Oman [18]. The reported production rate and disposal of OBM cutting is in the range of 300-500 t/day [19] and is expected to grow in the coming

years (Fig. 1). The three main storage sites for the cuttings are Elkhwair, Fahud, and Quran Al-Alam (Fig. 2).

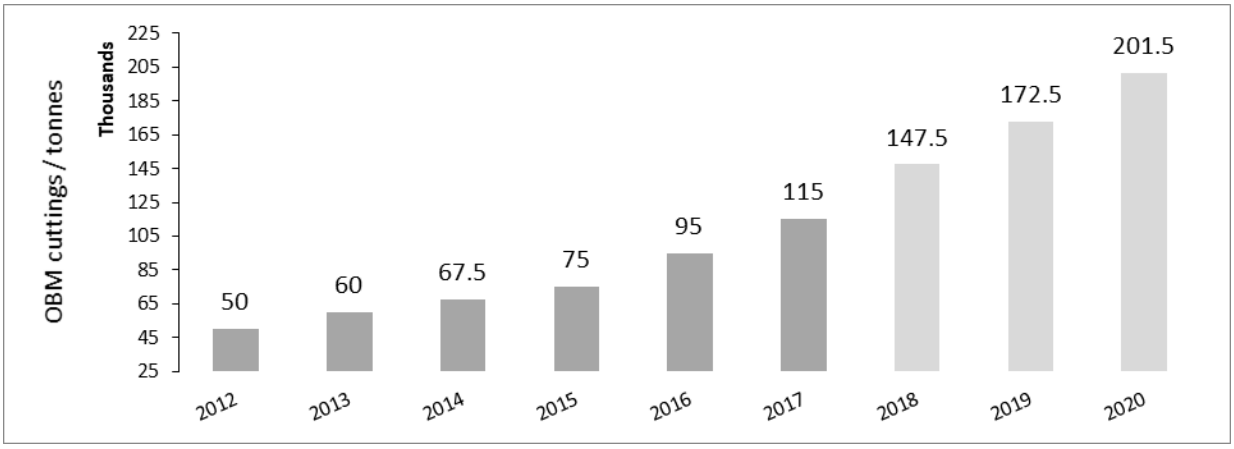

Fig. 1 Amount of OBM Cutting produced during oil-well drilling in Oman. Actual values are reported for 2012 to 2017; values from 2018 onwards are projected [18].

In Oman, only two integrated (clinkerisation + cement grinding) cement plants exist: the Oman Cement Company in the north, and the Raysut Cement Company in the south (Fig. 2). As of today, the total combined clinker production capacity in Oman is about 5 million t/year. This number is likely to increase to 6.8 million t/year by 2021 [20, 21]. When cement grinding plants are considered, the current total cement production is about 7.73 million t/year, with the capacity projected to increase to about 9.23 million t/year by 2021.

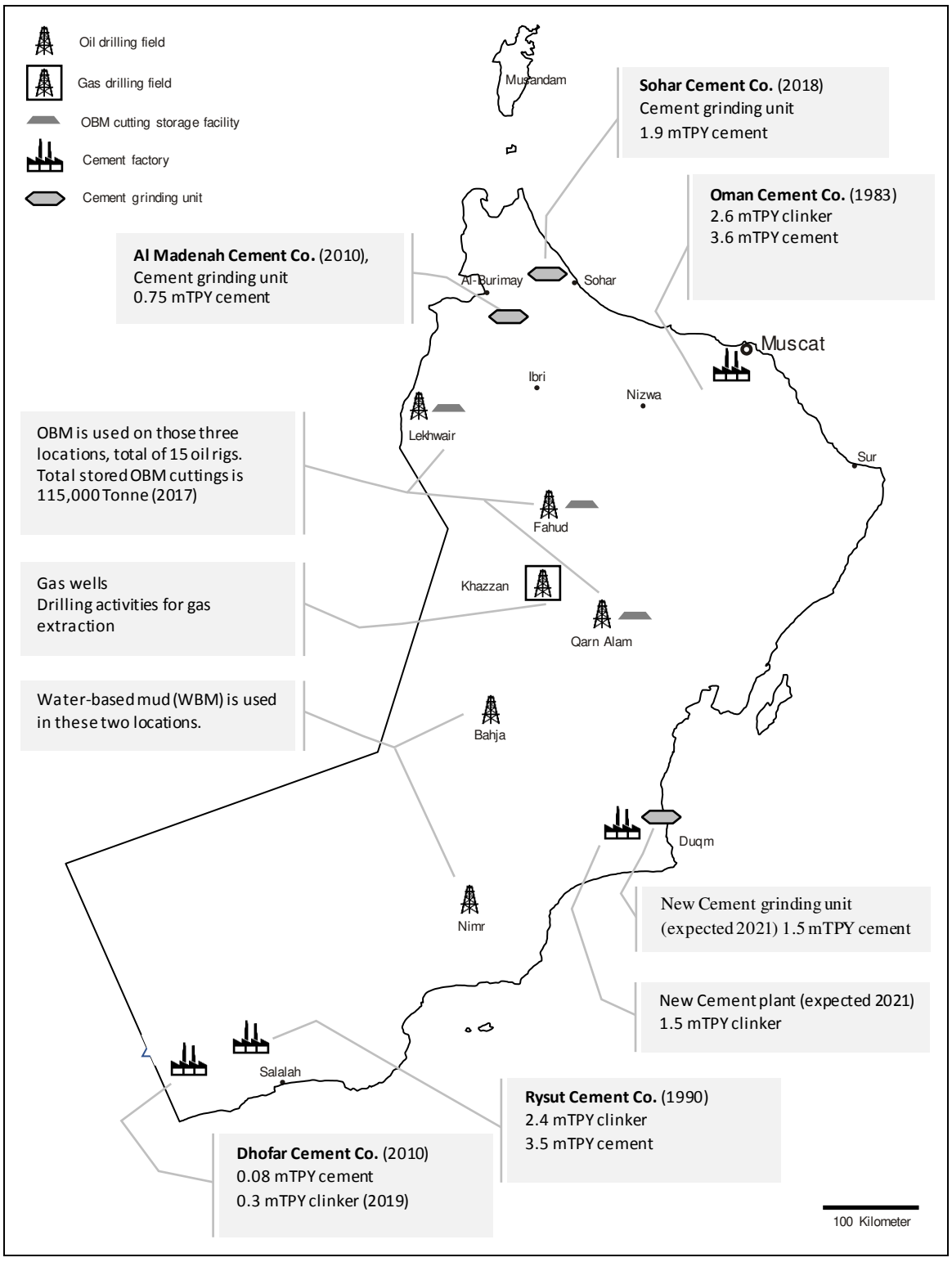

Fig. 2 Map of Oman showing the locations of oil fields and cement industries (the year of establishment is given in brackets) [19,20,22–24].

The extracted OBM cuttings cannot be used directly in cement manufacturing as some pre-processing is required. The OBM cutting from drilling operations is wet: it has high oil and water contents. The cutting is first transferred to an engineered landfill [9, 5], which is open, exposed to direct sunlight, and normally located in the desert. At this stage, the OBM cutting is simply left to dry under the effect of direct sunlight and high temperature. Within months, the moisture content decreases from 15-20% to about 10-8%, and the sludge is then transferred to a semi-dry lined pit. Air drying in direct sunlight continues for up to a couple of years, after which the moisture content is at most 5%. Currently, no accepted management solution exists for this waste; thus, the dried OBM cuttings often end up accumulating at the storage yard without additional processing.

The dry OBM sludge has the potential to be used as a component of cement raw meal for cement manufacturing. However, there are a number of different cements which could be produced using OBM cutting [25, 26], such as ordinary Portland cement or sulphate-resistant Portland cement. A number of studies have demonstrated the potential use of raw materials derived from demolished buildings in the cement industry [27-30]. In addition, the so-called “Oil Well Cement” (OWC) also has been reported in the literature [31–37].

2 Aim of the study

This study investigates the effects of the addition of OBM cuttings to the raw meal used in cement manufacturing, and reports on the properties of the so-obtained cement clinker.

3 Materials and methods

3.1 Raw mix design

Samples were prepared from dried OBM cutting blended with a number of raw materials used in the preparation of raw meal. The chemical composition of these materials is given in Table 1. These compositions of the blends were calculated to give the same phase composition as a real Portland cement clinker. Using the Bogue’s calculation, the amount of C_3S, C_2S, C_3A and C_4AF in raw meal after the heating process were calculated [38,39].

Table 1
Chemical composition of the raw materials used in this study

	Limestone	QPH	Kaolin	Iron Ore	OBM cutting
Main & minor oxides (% wt./wt.)					
SiO_2	3.60	76.30	41.28	18.28	20.90
Al_2O_3	0.55	9.20	33.27	10.32	4.74
Fe_2O_3	0.40	6.69	6.69	54.00	2.35
CaO	52.25	5.90	2.18	0.48	31.85
MgO	0.19	1.46	1.46	1.98	2.22
SO_3	0.04	0.26	0.18	0.12	1.81
K_2O	0.92	0.32	0.28	0.14	0.41
Na_2O	0.06	0.12	0.21	0.18	0.89
LOI @ 950 °C	41.59	2.42	14.15	9.98	32.70
Trace oxides (mg/kg)					
BaO	-	-	-	-	5500
Cr_2O_3	100	200	37000	100	100
MnO	100	1500	7600	100	300
Mn_2O_3	100	-	-	100	300
P_2O_5	600	900	200	200	1100
TiO_2	100	5400	4300	500	100

3.2 Raw meal samples (Rm)

Five raw meal mixtures were prepared by mixing different ratios of raw materials according to theoretical mix-design calculations. Raw meal samples were prepared with OBM cutting contents from zero (as a control sample) to 55%. A final sample was prepared from 100% OBM cutting, with no raw materials added. In addition, one sample of raw meal was obtained direct from a cement plant. This sample contained no OBM cutting and was identified as Rm_{ind} and later Ck_{ind}.

In addition to the prepared raw meal just mentioned, and to study the thermal behavior and obtain the clinker phases formation temperature in respect to different ratio OBM cutting added, an additional fourteen raw meal mixtures were prepared by mixing different ratios of raw materials according to the theoretical mix-design calculations with increasing OBM contents.

Table 2
The rawmix design

Raw Material	% Ratio				
	Rm_{Ind} Zero OBM	**$Rm_{Ref.}$** Zero OBM	**Rm12** 12% OBM	**Rm55** 55% OBM	**Rm100** 100% OBM
Limestone	81.40	80.90	72.60	43.00	-
Quartzo-phillite	12.32	11.35	8.60	-	-
Kaolin	4.35	5.65	4.70	0.50	-
Iron ore	1.93	2.10	2.10	1.50	-
OBM cutting	-	-	12.00	55.00	100.00
Total	100.00	100.00	100.00	100.00	100.00

3.3 Clinker samples (Ck)

Nodules of about 5-8 mm size were prepared from the raw meal by adding water [40]. The dried raw meals were fired using a platinum dish in a static air high-temperature furnace (Carbolite, model RHF 16/3). The clinker was prepared according to Al-Dhamri et. al [41].

3.4 XRF and XRD

Clinker samples were characterized using a PANalytical Axios Fast XRF spectrometer.

Sample phases composition were determined using a CubiX PANalytical diffractometer, with Cu Kα radiation operating at 45kV and 40 mA. The measurements were performed over a 2θ range from 10° to 65° with a scanning rate of 0.021° per second and a step time of 14 seconds, with full run lasting for 50 minutes. The crystalline phases were identified and refined using the HighScore© program from PANalytical.

3.5 Loss on ignition test (LOI) and free lime test

LOI was determined by igniting a known mass of the sample at 950 °C [42]. The percentage of free lime was obtained by refluxing a known quantity of ground clinker (about 1 g) in an alcoholic solution of ammonium acetate. The mixture was filtered and titrated with 0.04 M EDTA [43,44].

3.6 Inductively Coupled Plasma (ICP-OES)

The raw materials and the clinker samples were analysed to determine trace element and heavy metal contents. The digested sample was analysed for metals oxides using an inductively coupled plasma optical emission spectrophotometer (ICP-OES) analytical instrument (Agilent 5110 SVDV) with nebulizer flow of 0.70 L/min, plasma flow 12.0 L/min, Stabilization time 6 seconds and 1.20 kW power.

3.7 SEM-EDX

This was used to identify clinker phase formation temperatures, by scanning samples under SEM-EDX that had been burned at temperatures from 1180 ^{o}C up to 1500 ^{o}C. The method was also used to detect trace elements in the different clinker phases. The polished cross-sections were studied in backscattered scanning electron (BSE) mode using a Carl Zeiss EVO MA15 SEM at 15 kV with a working distance of 8 mm, while 20 kV was used for the elemental mapping.

3.8 DSC-TGA

Differential scanning calorimetry and thermogravimetric analysis (DSC-TGA) of the raw meals (RM_{ind}, $RM_{Ref.}$, RM12, RM55 and RM100%) were performed using a DSC-TGA Universal V4.5A TA Instrument at heating rate of 10 ^{o}C/min, under normal atmospheric condition from 20 ^{o}C to 1450 ^{o}C [46].

3.9 Burnability test

The burnability test was conducted by sintering in laboratory furnace for 45 minutes at five different temperatures (1300, 1350, 1400, 1450 and 1500 ^{o}C) [47,48].

4 Results and Discussion

4.1 Mineral Composition

The main clinker phases in all clinker samples are formed such as alite (C_3S), belite (C_2S), tricalcium aluminate (C_3A) and ferrite (C_4AF). The concentrations of alite and belite versus OBM cutting content is reported in Fig. 4. This figure shows the results from both Rietveld refinement of the XRD patterns and the theoretical calculations based on Boque equations (Table 3).

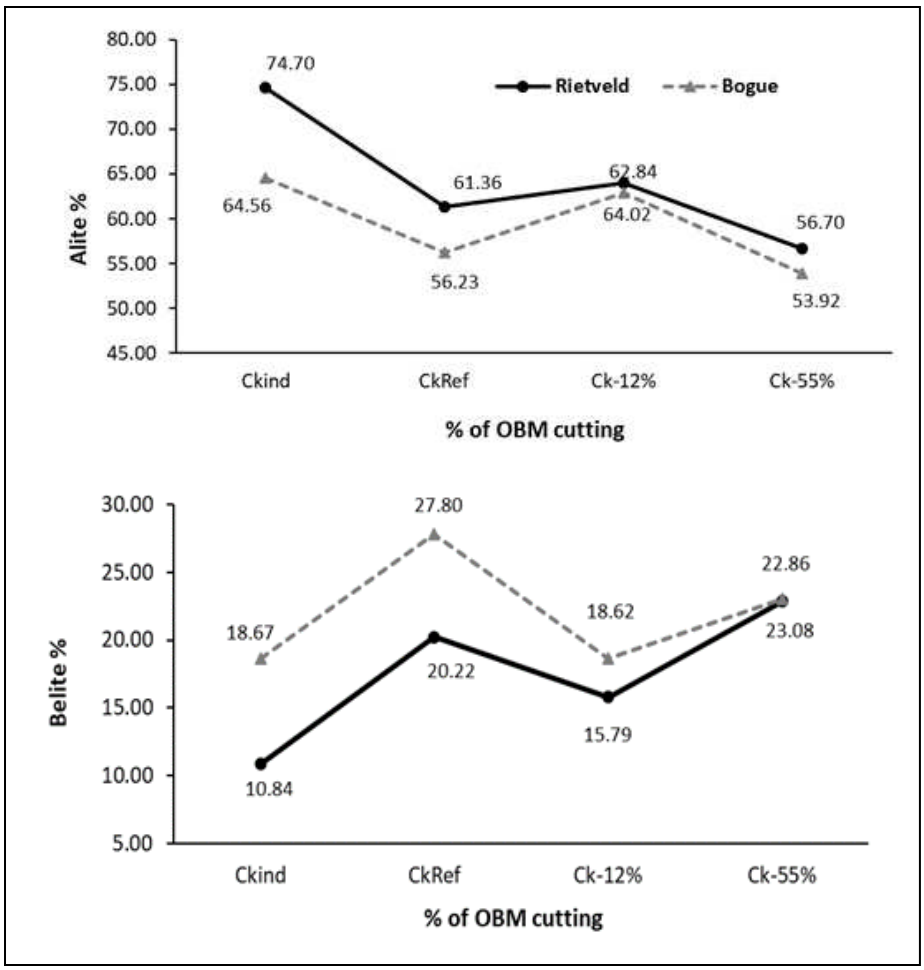

Fig. 3 XRD patterns of the prepared clinker

There was no discernable change in alite or belite polymorph with OBM cutting content (Fig. 3). However, the levels of alite and belite formed was dependent on OBM cutting content (Fig. 4). This had not been especially predicted by the Bogue calculations, but the Rietveld refinement data showed a gradually decreasing alite content (and corresponding increasing belite content) with increasing OBM cutting content. Indeed, it is noteworthy that the Bogue calculations underestimated the alite content and overestimated the belite content at OBM cutting contents of up to 5%.

While the industrial clinker showed the highest levels of alite, addition of OBM cutting to the reference raw meal led to increased alite contents. It was not until the OBM cutting level was over 15% that the alite content dropped below that observed for Ck_{ref}. These

differences could be explained while exploring the other parameters such as influence of trace elements content, raw materials characterization and OBM cutting behaviour.

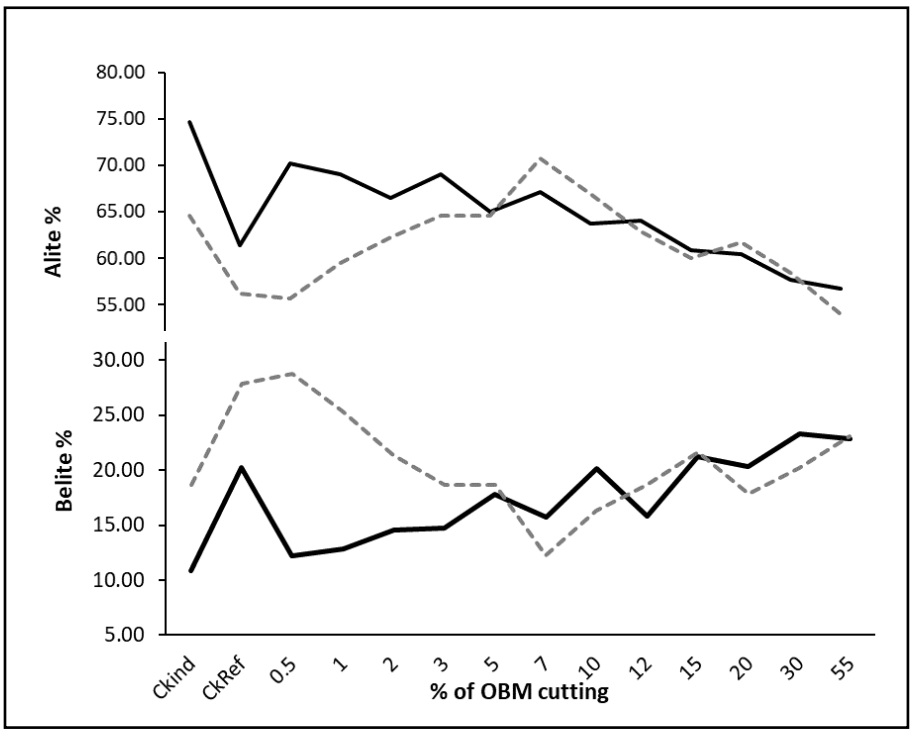

Fig. 4 Clinker phases concentrations by XRD Rietveld analysis (represented by full black line) and by Bogue equation (represented by gray dotted line)

Table 3
Chemical oxide and clinker phases composition of the prepared clinker

	$Ck_{ind.}$	$Ck_{Ref.}$	Ck-12%	Ck-55%	Ck-100%
Major oxides (% wt./wt.)					
SiO_2	22.19	22.58	21.79	21.88	32.49
CaO	65.45	65.32	65.87	65.68	51.55
Al_2O_3	4.06	5.46	5.37	5.02	7.82
Fe_2O_3	4.07	3.86	3.82	3.88	3.88
LOI @950 °C	0.25	0.12	0.07	0.06	0.04
Minor oxides (% wt./wt.)					
MgO	1.53	0.81	1.24	1.43	1.66
SO_3	1.40	0.30	0.83	1.57	0.33
Na_2O	0.25	0.32	0.35	0.34	0.20
K_2O	0.39	0.25	0.07	0.02	0.11
Trace oxides (mg/kg)					
BaO	-	-	2300	8500	11500
Cr_2O_3	1200	1100	700	600	500
MnO	400	500	400	400	400
P_2O_5	900	1200	1100	1200	1200
TiO_2	2400	3200	2800	2000	2000
Clinker Module factors & phases (%)					
the phases calculated according to Bogue equations [52,53]					
LSF	92.53	90.5	94.33	94.22	48.45
SM	2.46	2.42	2.37	2.46	2.95
AM	1.22	1.41	1.41	1.29	2.02
C_3S	64.66	52.06	60.97	61.78	-
C_2S	14.93	25.55	16.57	16.21	<36.63
C_3A	3.87	7.94	7.77	6.74	14.16
C_4AF	12.39	11.75	11.62	11.81	11.80

4.2 $CaCO_3$ decomposition

Thermal analysis of various raw meal samples showed that the calcination temperature decreased with OBM cutting content. Calcite decomposition occurred at 817 ^oC when no OBM was in the sample, falling consistently with increasing OBM cutting content until the OBM cutting alone (Rm100%) showed decomposition at 763 ^oC. The greater than 50 ^oC difference in decomposition temperature between limestone and OBM cutting is of interest. To understand why the addition of OBM cutting reduces the calcination temperature, it is important to study the nature of the calcite in OBM cutting and compare it with that in the limestone.

Many studies [54–58] have reported the limestone reactivity and linked it to the calcite structure. Different grain sizes [59] and impurities within the limestone can cause variations in the limestone's textural and mineralogical properties, and subsequently influence the calcination temperature [60]. This may also influence both the crystallization temperature in different phases of the clinker formation and free lime content in the produced clinker [61,62]. It has also been reported that the presence of dolomite in limestone helps speed up the calcite decomposition rate [62].

In 1962, Dunham [63] established a systematic classification scheme for carbonate sedimentary rocks. Initially known as the "Dunham Classification", this was later modified by Embry and Kloven [64–66] to include coarse-grained limestone and became known as the "Modified Dunham Classification". This has become the most commonly used classification in petrographic thin sections for identifying and distinguishing different types of limestone based on the grain-size, ratio, shape and microstructure.

The Dunham classification divides limestone into six sub-classes based on the presence or absence of mud supporting the carbonate grains, the grain content and nature of the matrix during deposition. The limestones may be further defined by two sub-groups: 1) grain-supported limestone and 2) mud-supported limestone. This division depends on the percentage of the grains (known as allochems) or mud matrix (known as orthochems). The grain-supported limestone is characterized by texture with

little or no lime mud but an abundant framework of grains that support each other, while the mud-supported limestone consists of grains floating in a muddy, mainly calcitic, matrix [67].

Analysis of petrographic thin sections of the limestone used here shows calcite crystals of a depositional texture, with no regular shape and unevenly distributed without common direction, (Fig. 5). The grains are coarse (>3mm) and compacted with no void space between calcite crystals, appearing flat and with some fractures. This limestone could be classified as crystalline limestone according to the Dunham classification [63].

The OBM cutting meanwhile showed a different petrography, with the calcite being mud-supported, with loose packed grains and high porosity. The clay grains were mostly present as developed clusters and were immersed in oil. Lath shaped plagioclase grains with sharp grain margins were also present, as shown in Fig. 5c and Fig. 5d. The calcite showed round sub-millimeter grains, which were highly brittle and fragile in nature. Later XRD analysis of OBM cutting showed the presence of dolomite. Therefore, classification of the OBM cutting could be a mix between two or three types of limestone, falling between mudstone and wakestone. However, the classification certainly showed a difference from the limestone used in this research.

These differences help to explain the lower decomposition temperature of OBM cutting compared to limestone. Firstly, the OBM cutting contained dolomite, while none was present in the limestone. Dolomite in limestone lowers the decomposition temperature of the calcination process. Marinoni et al. [68] showed that limestone decomposition starts with the rapid dissociation of dolomite in the first few minutes, followed by calcite decomposition. Dolomite dissociation occurs in a single step, without a calcite intermediate phase. This suggests that the presence of dolomite reduces the calcination activation energy [61,62,68]. Marinoni et al. [62] proposed that limestone dissociation starts with dolomite decomposition, resulting in the formation of grain cracks due to the $CaMg(CO_3)_2$ structure, increasing the surface area and so allowing CO_2 diffusion [57,62,69].

The lower decomposition temperature in OBM cutting may also be related to the calcite texture therein, which differs from the calcite in limestone, as explained above. Finally,

the OBM cutting is more porous than the limestone, allowing more surface area for heat transfer. As seen petrographically, the calcite grains float in the mud, with larger spaces between grains than in the limestone (Fig. 5c and 5d).

Similar results were obtained by Marinoni et al. [62] and Galimberti et al. [61] when studying the thermal decomposition and burnability of limestone used for manufacture of industrial cement clinker. Using different limestone sources revealed that the texture of mud-supported limestone had a strong impact on the calcite decomposition temperature and its decomposition rate. According to the Dunham calcite classification [65,66], raw meal where the limestone is of grain-supported origin is more reactive.

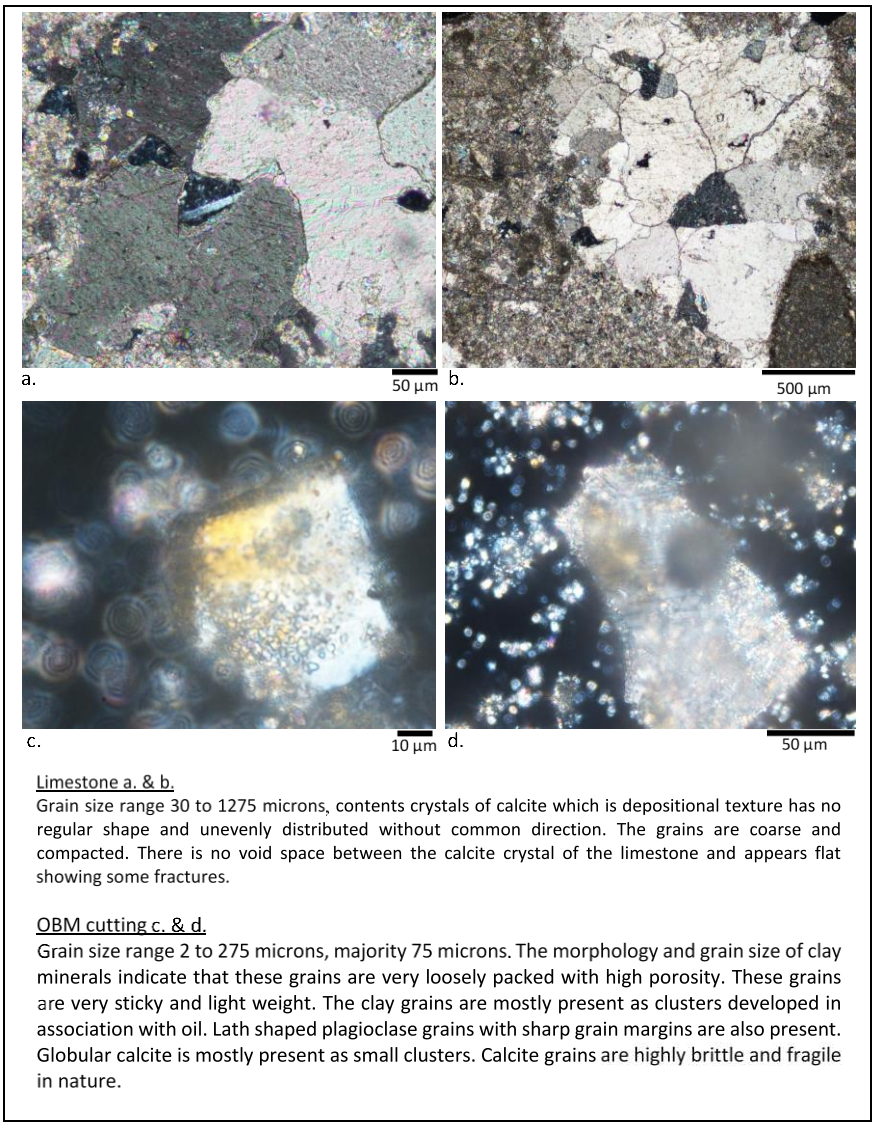

Fig. 5 Limestone and OBM cutting petrography analysis

The calcite grain size also has an effect on both the rate of decomposition and the temperature at which decomposition occurs. Coarser grains show higher decomposition temperatures and lower rates of decomposition [70], as illustrated in Table 4.

Table 4
Effect of calcite grain size on dissociation of limestone (according to Chatterjee [70])

Crystallinity	Grain size, mm	Relative rate of dissociation	Relative dissociation temperature
Very coarse grained	> 1.00	Lowest	Highest
Coarse grained	1.00 – 0.50		
Medium grained	0.5 – 0.25		
Fine grained	0.25 – 0.10		
Very fine grained	0.10 – 0.01		
Microcrystalline	< 0.01	Highest	Lowest

The effect of particle size was confirmed by grinding the limestone for 5 minutes and then obtaining two fractions; that passing a 212 micron sieve and that passing a 63 micron sieve. These two fractions were compared against ground OBM cutting passing through a 212 micron sieve. The particle size distributions of the three resultant materials were comparable to materials used in a cement plant and are shown in Fig. 6, together with TGA analysis of the three samples. The finer limestone decomposed at a lower temperature than the standard limestone, with OBM cutting decomposing at a lower temperature still. Thus, the lower decomposition temperature of the OBM cuttings may be explained by the finer calcite grains (Fig. 5c and 5d) and the presence of dolomite. The calculated activation energies (E_a) of $CaCO_3$ decomposition for limestone and OBM cutting are 154.43 $J.mol^{-1}$ and 181.46 $J.mol^{-1}$ respectively (Fig. 7), confirming the observations made by Chatterjee et al. [70].

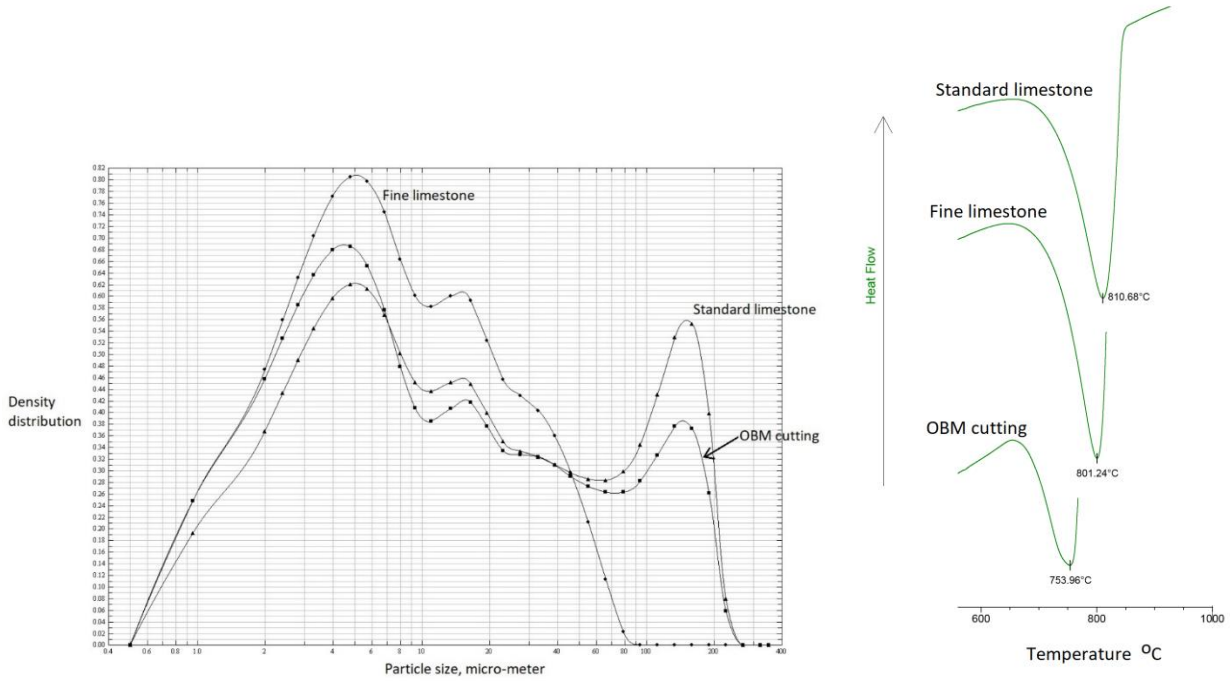

Fig. 6 Particle size distribution and decomposition temperature of: 1) fine limestone, 2) limestone, and 3) OBM cutting

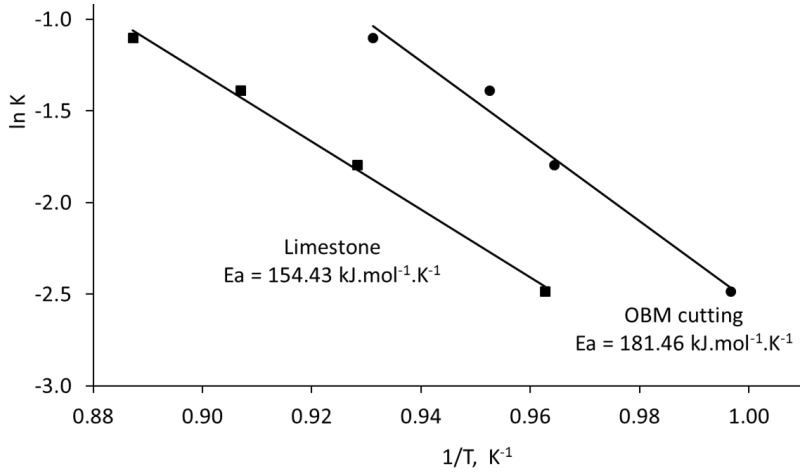

Fig. 7 Activation energy value of $CaCO_3$ decomposition reaction in limestone and OBM cutting

4.3 Burnability

Fig. 8 shows the burnability data obtained in this study. Fig. 8a shows the data obtained from cement industry raw meal ($Rm_{Ind.}$) and the reference raw meal prepared in the laboratory ($Rm_{Ref.}$). The free lime content for both mixes fell with increasing temperature. However, the free lime content of Rm_{Ind} was always greater than that of Rm_{Ref}, with the difference between the two decreasing with increasing temperature, until the difference was minimal at 1400 ^{o}C and above. The higher free lime content for Rm_{Ind} could be due to its higher LSF, i.e. 92.53 compared to 90.50 for Rm_{Ref} (see Table 3). Thus, there is more CaO to be consumed during clinkering. This is supported by the convergence of the two data sets with increasing temperature. Both mixes showing similar burnability behavior validates the use of the reference raw meal in comparisons with raw meal prepared using OBM cutting.

Fig. 8b shows the burnability results for Rm_{Ref} plus raw meal prepared using 12%, 55% and 100% OBM cuttings. Despite the falling free lime contents with increasing temperature, there was an increase in free lime with increasing OBM cutting content, suggesting harder burnability. However, this did not apply to the sample prepared from 100% OBM cutting. This sample showed very easy burning behaviour (Fig. 8c). The free lime dropped significantly, even at 1300 ^{o}C (0.2% free lime), then showing only 0.02% free lime content when heating at 1500 ^{o}C. However, as shown by XRD analysis (Fig. 9), when burned at 1200 ^{o}C, the 100% OBM cutting showed belite formation and a very low free lime content. Higher temperatures still led to no alite formation due to there being no CaO remaining as shown in Fig. 13d. This was confirmed by SEM-EDX analysis (Fig. 10), where no alite was observed. The absence of alite can easily be understood in terms of the LSF, which at 48.45 was considerably lower than for all of the other samples.

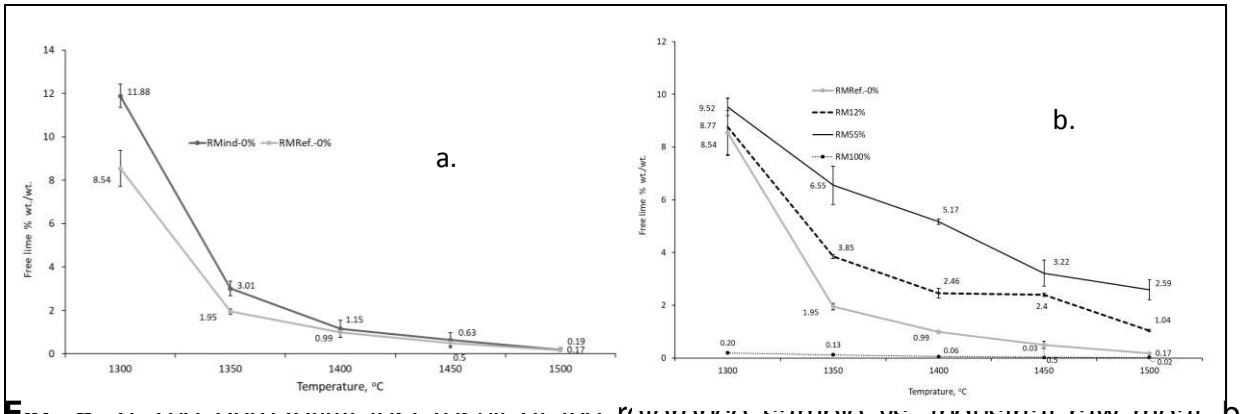

Fig. 8 a) The burnability test result of the reference sample vs. industrial raw meal. b) The burnability test of the reference sample vs. raw meals with 12%, 55% and 100% OBM cutting

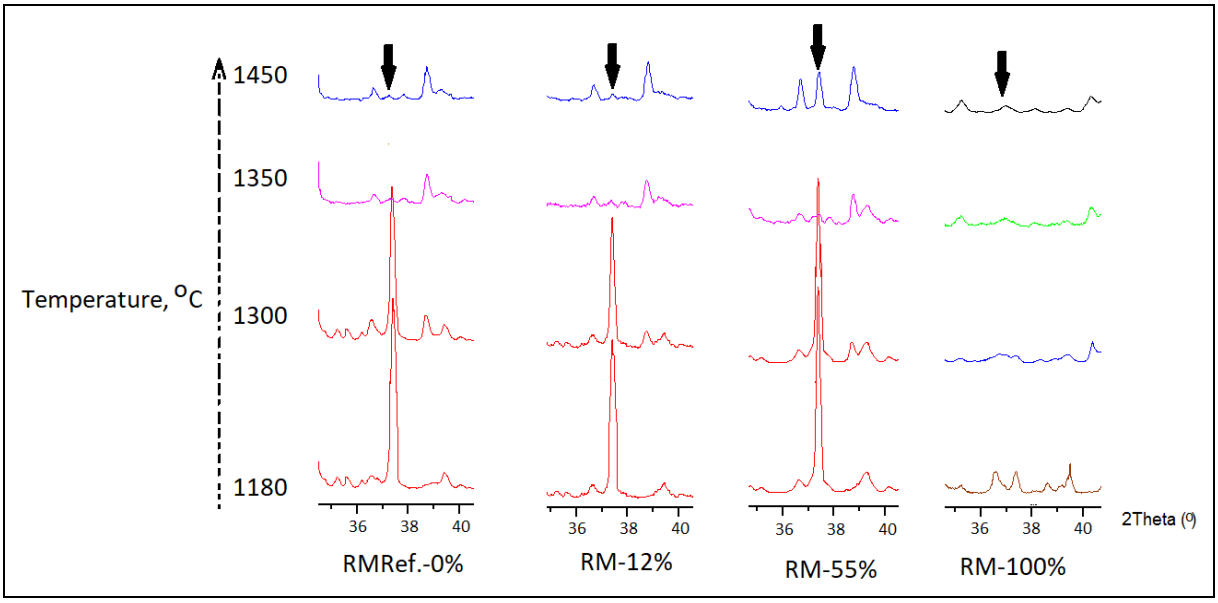

Fig. 9 XRD pattern of the different raw meal samples burned at different temperatures, the arrows show the free lime peak at 2theta = 37.36º.

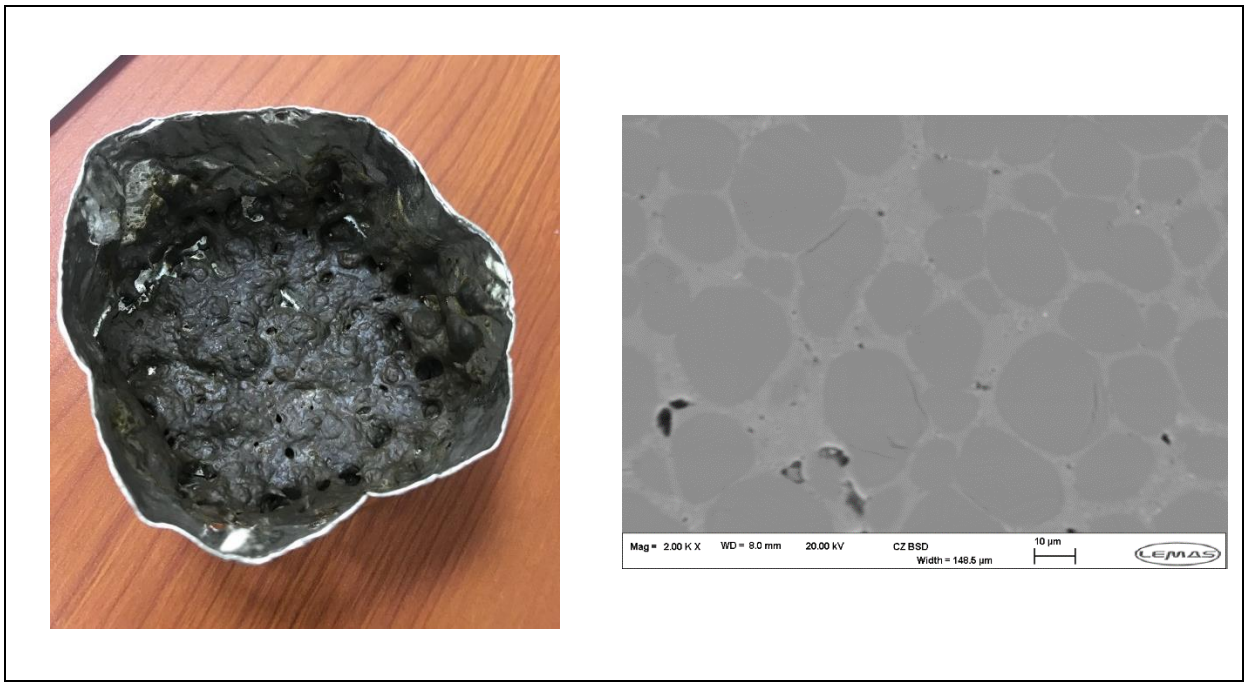

Fig. 10 Left: clinker sample (100% OBM cutting) after burning at 1450 ºC in platinum crucible for 30 minutes. Right: SEM analysis of the same clinker sample on the left

4.4 The XRD and TGA

XRD and TGA were used to measure clinker phase composition and obtain information on the changes in clinkerization during the heating process. Thermal analysis (Fig. 11) showed that all of the changes occurring during the heating process, including $CaCO_3$ decomposition, belite formation, liquid phase and alite formation (liquid phase sintering) shifted to lower temperatures as the OBM cutting content of the raw meal increased.

The effect of OBM cutting on $CaCO_3$ decomposition temperature was described earlier, but the effect on other phases is described below. At higher temperature (above 1338 ^oC) [71] the liquid phase develops. This comprises mainly Al_2O_3 and Fe_2O_3 bearing phases. These are essential fluxes, lowering the energy required for completing the clinkerization process. When melting commences, the liquid content can increase significantly, up to 15 – 25% [71]. The presence of other minor oxides such as SO_3, MgO and alkalis can have an influence by lowering the energy required to form the flux. In this study RM_{Ind} showed the presence of a liquid phase from 1334 ^oC, very close to temperature of liquid phase reported in the literature [71]. However, Rm_{Ref} showed temperature of formation of the liquid phase from 1331 ^oC which also close to industrial sample. However, with increasing OBM cutting content, the liquid phase formed at ever

lower temperatures, decreasing to 1320 °C with 55% OBM cutting and 1263 °C when 100% OBM cutting was clinkerized. This could be attributed to the present of minor oxides from the OBM cutting, as shown in Table 3 and Fig. 12.

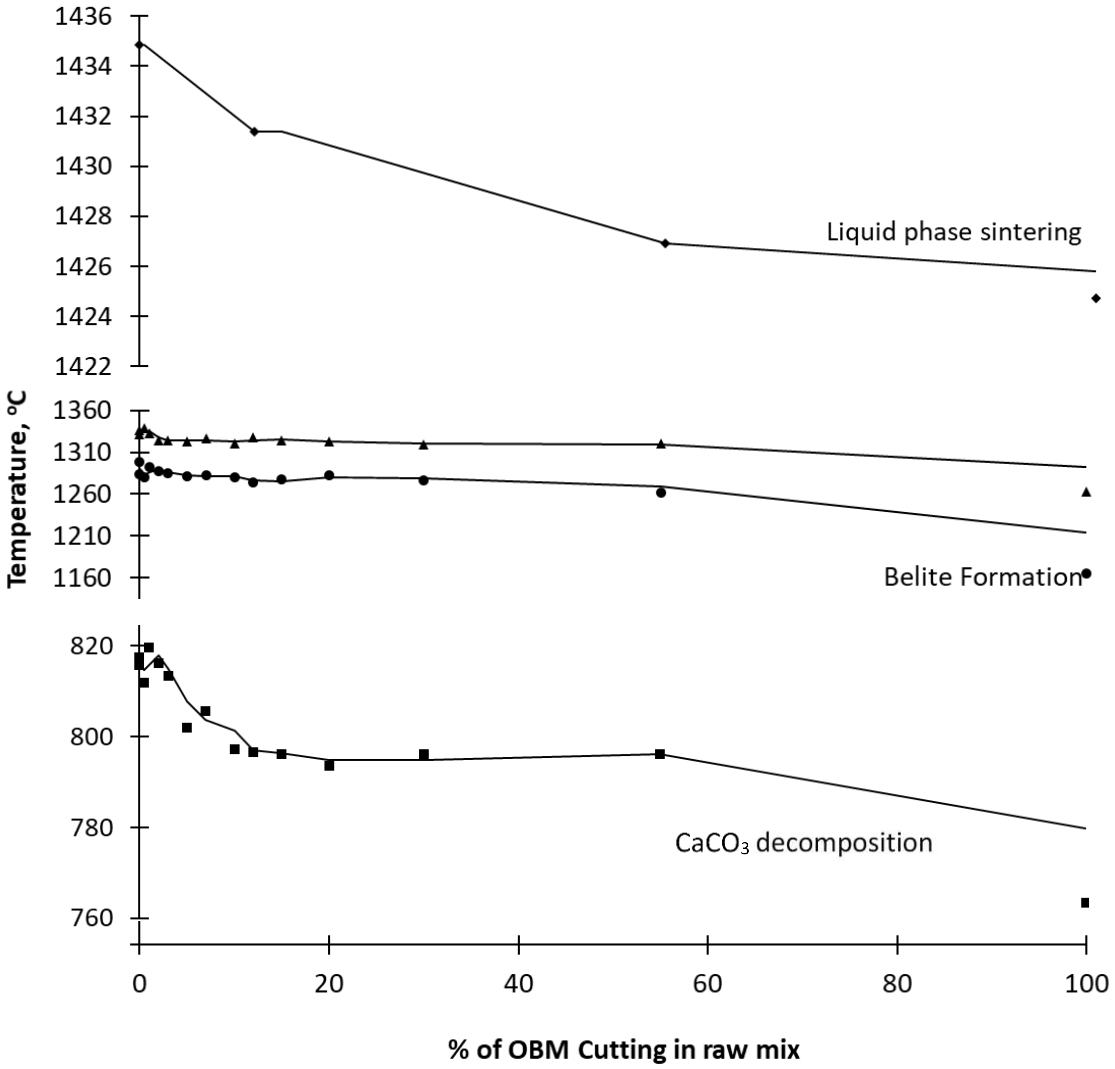

Fig. 11 Calcination temperature and the temperature of main phases of the clinker formation of raw meal with increasing % of OBM cutting which is obtained from the DTA analysis (the trend lines are moving average trendline)

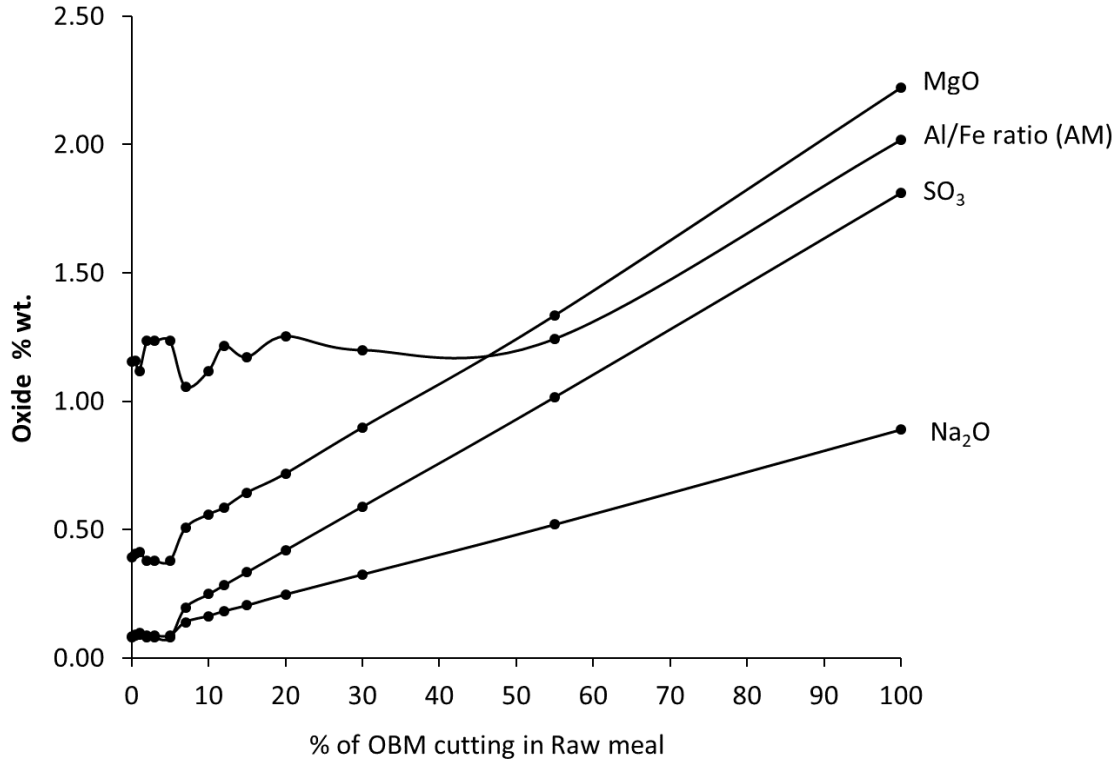

Fig. 12 Minor oxides content in prepared clinker

The decreasing temperature for the onset of liquid phase formation with increasing OBM cutting content also influenced the sintering temperature. The role of the liquid phase at this stage is very important and critical to the clinkerization mechanism. The liquid wets the solid grains, forming an interpenetrating film [71]. This has two main functions: 1) its surface tension pulls the solid grains together, serving to form clinker nodules. 2) It also eases transport of the main oxides in the liquid phase during the sintering stage and aids formation of alite and belite. The lower temperature for the onset of liquid phase formation, due to the presence of the minor oxides, impacts also on the sintering temperature, which were too close for Rm_{Ref} and Rm12 at 1434 ^{o}C and 1431 ^{o}C respectively. However, the sintering temperature fell to 1424 ^{o}C for Rm55.

The clinker sample made with 100% OBM cutting, CK100%, showed formation of belite at 1200 ^{o}C, as indicated by XRD and SEM-EDX analysis. At higher temperatures, no further new phases were formed. The CK-100% at 1450 ^{o}C showed belite grains

swimming in a high melt content (Fig. 10), a result of the high concentration of Al_2O_3 and Fe_2O_3 % in the mix.

4.5 The Effect of Barium on clinkerization

As shown above, the incorporation of OBM cutting had a slight, yet noticeable effect on clinker composition. Initial elemental analysis of the raw materials showed that a number of trace elements were present in the OBM cuttings (Table 1), while the presence of some trace elements plays a major role on clinker phase formation [72–79]. This was thus investigated further, with particular focus on the barium content.

In Rm_{Ref}, the belite and alite formation temperature was 1284 and 1331 °C respectively, but these fell upon incorporation of OBM cutting. SEM-EDX and and ICP analysis (Table 5) both showed an increase in barium content with increasing OBM cutting content. Furthermore, SEM-EDX analysis revealed the distribution of barium through the clinker phases. The highest barium concentration was found in the liquid phase.

Table 5
BaO content in clinker phases (mg/kg)

Sample	Ck_{Ind}	$Ck_{Ref.}$	Ck12	Ck55	Ck100
Alite	-	-	3500	4200	-*
Belite	-	-	2500	19800	64000
Liquid phases	-	-	25700	24600	143200

*no alite observed in Ck100.

The effect of barium on phase composition is related to the free lime content. An increased free lime content indicates reduced burnability and incomplete formation of the main clinker phases. This is possibly due to alite formation being destabilized. As stated earlier, the addition of OBM cutting decreased burnability and the free lime contents increased (Fig 13). With the OBM cutting containing 0.85 wt% BaO, the barium content of the clinker increases with increasing OBM cutting content. It has repeatedly been shown that BaO has a negative influence on alite formation, thus increasing the free lime content. Kolovos et al. [74,80] studied the effect of raw meal BaO content on

the reactivity of the $CaO\text{-}SiO_2\text{-}Al_2O_3\text{-}Fe_2O_3$ system. They noticed that the addition of 1% BaO to the raw meal then sintering at 1200 °C and 1450 °C led to an increase in free lime compared with the reference sample. This BaO was then shown, by SEM analysis, to concentrate in the melting phase of the clinker.

Other studies [74,81-84] have also reported on the impact of barium on clinkerisation reactions. These mostly confirm that the free lime content increases with barium content, and that barium is mainly concentrated in the melting phase. Furthermore, Zezulova et al. [81], in addition to showing high BaO contents in the melting phase, also reported higher concentrations of BaO in belite than alite. This is possibly caused by the crystal lattices of alite and belite, with the belite structure being more accommodating of foreign ions [81].

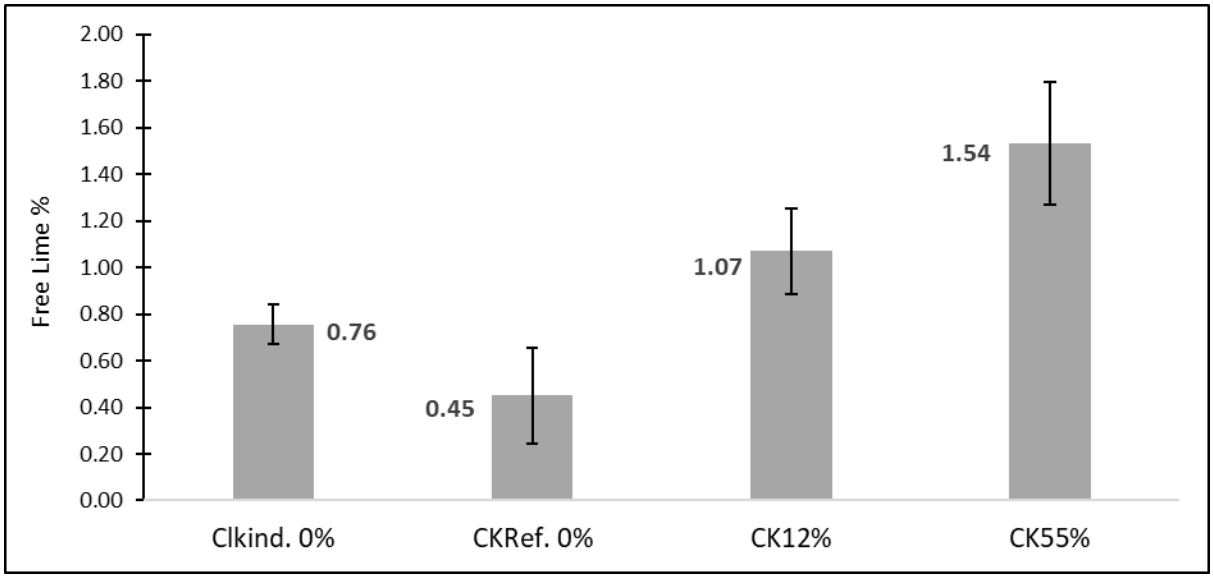

Fig. 13 The free lime content for each clinker sample

Clinker morphology and chemical composition was then studied by SEM/BSE imaging and EDX analysis. Below 1250 °C, clinkerization proceeded through solid-solid reactions, in the absence of the liquid phases. These reactions occurred at the original phase boundary between the solids [85], leading to the formation of belite, see Fig. 14A1. This happens through diffusion of the CaO on the SiO_2 surface as could be seen in the SEM-EDX in the reference clinker sample $Ck_{Ref.}$ and the industrial sample Ck_{Ind} which are shown in Fig. 14A1 and 14B1. EDX analysis revealed a cluster of SiO_2

surrounded by the CaO. This led to belite formation, which is known to form between 900 ^{o}C and 1250 ^{o}C [86,87] with the precise formation temperature defined by a number of factors, such as minor compounds [72,74,76,79,88,89], particle sizes [90] and retention time [40].

The raw meal containing 12% OBM cutting showed some formation of alite at 1350 ^{o}C (Fig. 14A1). Free lime was present in clusters, but belite was not observed. The co-existence of alite and free lime without belite suggest that no further alite could be formed, irrespective of temperature, because no belite is available to react with any free lime. Fig. 15 shows the SEM images with EDX mapping for Ck100% heated at three different temperatures; 1300, 1350 and 1400 ^{o}C. At all temperatures, belite was the dominant phase, showing rounded to regular edges. XRD patterns from Ck100% heated to 1000 ^{o}C showed formation predominantly of belite, plus free lime (Fig. 16). However, upon heating to 1300 ^{o}C there was no evidence of free lime in either the XRD patterns nor the SEM images. The same was observed when the temperature was raised further, to 1350^{o}C. While temperatures above 1400 ^{o}C would normally be expected to yield alite, the lack of free lime in the Ck100% sample meant that alite formation was not expected. XRD analysis confirmed the absence of alite. Finally, EDX mapping revealed the concentration of magnesium and barium in the liquid phase, at all temperatures (Fig. 17B1 and 17B2), with the formation of C_3A and ferrite.

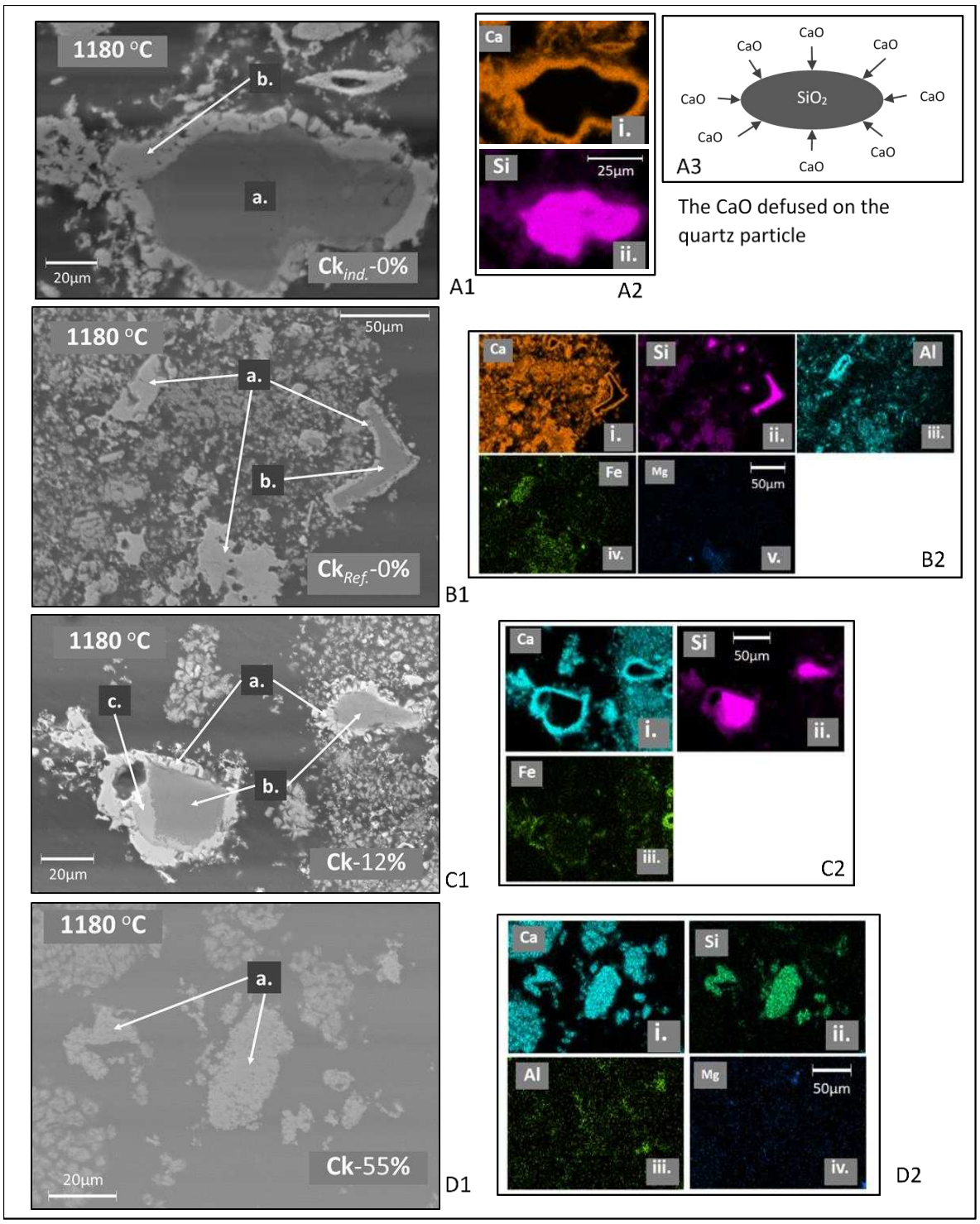

Fig. 14 Microstructure of clinker samples analysis.

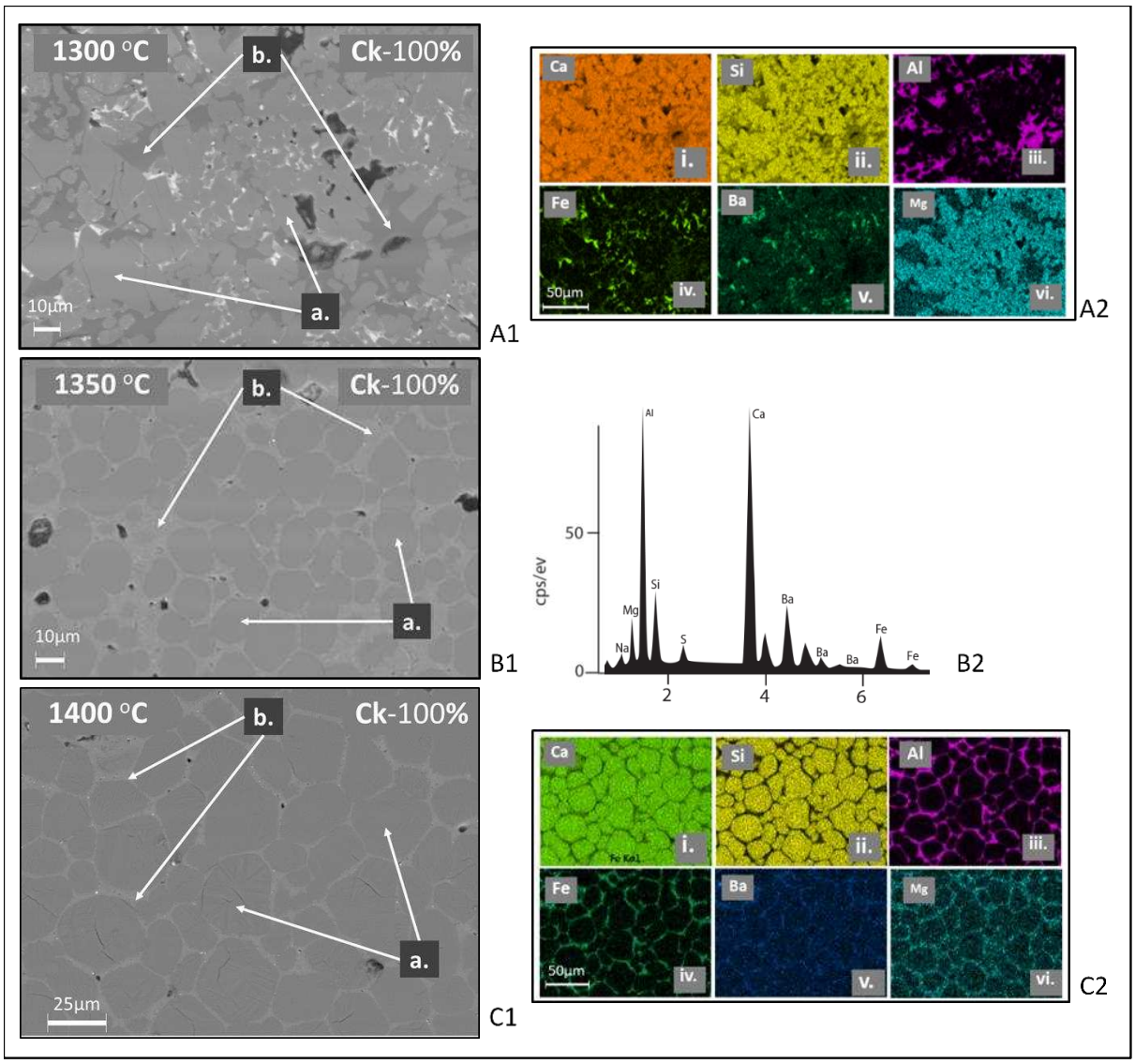

Fig. 15 Microstructure of clinker samples analysis that prepared by 100% OBM cutting

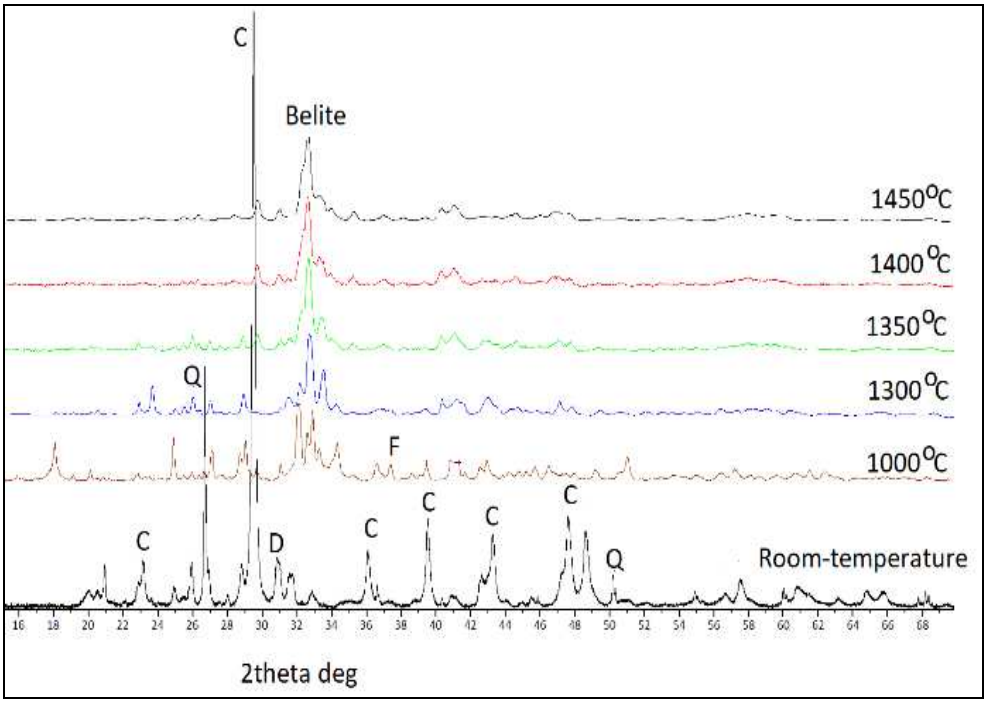

C: Calcite, D: Dolomite, F: free lime, Q: Quartz

Fig. 16 XRD of OBM cutting heated to different temperatures

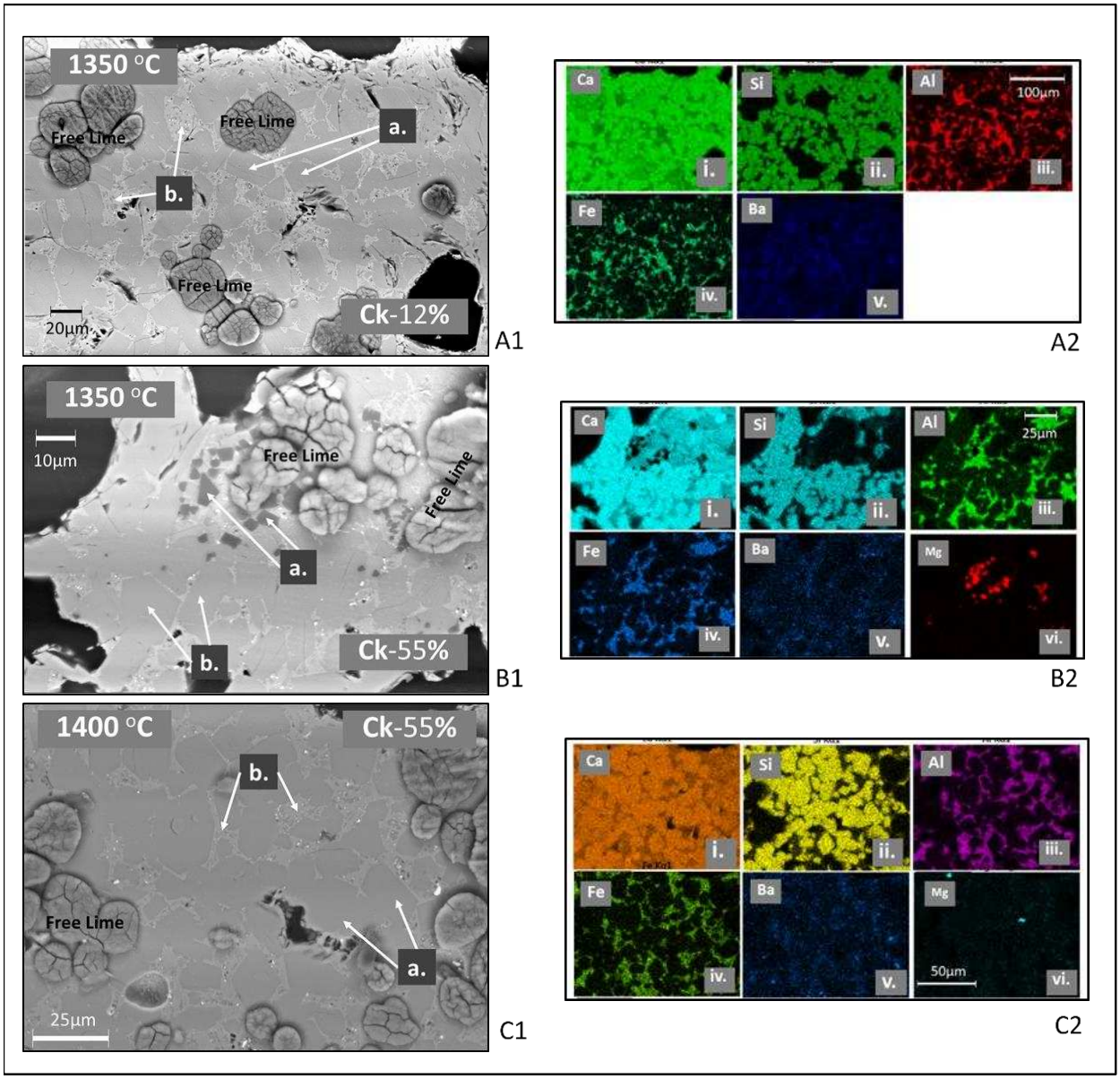

Fig. 17 Microstructure of clinker samples analysis

5 Conclusions

The results presented in this study demonstrate that the clinker prepared using OBM cutting has very similar properties to those of the clinker prepared from limestone normally used in cement production. This implies that OBM cutting could be recycled in the manufacturing process of Portland cement clinker. More in detail, the main results of this study are listed as follows:

- The addition of OBM cutting lowers the calcination temperature. This is because the calcite in OBM cutting has a smaller grain size than that in limestone.
- Furthermore, the OBM cutting contains some dolomite ($CaMg(CO_3)_2$). This increases the rate of carbonate dissociation, thus contributing to lowering the calcination temperature.
- However, the addition of OBM cutting to the raw meal leads to a higher free lime content in the resulting clinker. This can have several causes. In this work, the role of trace elements, especially barium, in destabilizing alite has been demonstrated.

  Clinker could be prepared simply by heating the OBM cutting at 1200 °C, without any additives. The XRD and SEM-EDX analysis of the resulting clinker showed the formation of belite with a very low free lime content, and no alite formation.

6 Funding and Acknowledgements

This work is part of a PhD programme at the University of Leeds, UK which is funded by Oman Cement Company, Sultanate of Oman (www.occ.om).

7 References

[1] R. Caenn, G. V. Chillingar, Drilling fluids: State of the art, J. Pet. Sci. Eng. 14 (1996) 221–230. doi:10.1016/0920-4105(95)00051-8.

[2] M.S. Al-Ansary, A. Al-Tabbaa, Stabilisation/solidification of synthetic petroleum drill cuttings, J. Hazard. Mater. 141 (2007) 410–421. doi:10.1016/j.jhazmat.2006.05.079.

[3] S.A. Leonard, J.A. Stegemann, Stabilization/solidification of petroleum drill cuttings: Leaching studies, J. Hazard. Mater. 174 (2010) 484–491. doi:10.1016/j.jhazmat.2009.09.078.

[4] J.M. Davies, J.M. Addy, R.A. Blackman, J.R. Blanchard, J.E. Ferbrache, D.C. Moore, H.J. Somerville, A. Whitehead, T. Wilkinson, Environmental effects of the use of oil-based drilling muds in the North Sea, Mar. Pollut. Bull. 15 (1984) 363–370. doi:10.1016/0025-326X(84)90169-3.

[5] S.M. Almudhhi, Environmental impact of disposal of oil-based mud waste in Kuwait, Pet. Sci. Technol. 34 (2016) 91–96. doi:10.1080/10916466.2015.1122630.

[6] J.P. Robinson, S.W. Kingman, C.E. Snape, R. Barranco, H. Shang, M.S.A. Bradley, S.M. Bradshaw, Remediation of oil-contaminated drill cuttings using continuous microwave heating, Chem. Eng. J. 152 (2009) 458–463. doi:10.1016/j.cej.2009.05.008.

[7] S.X. Xie, G.C. Jiang, M. Chen, Z.Y. Li, X.B. Huang, C. Liang, X.P. Jia, Harmless treatment technology of waste oil-based drilling fluids, Pet. Sci. Technol. 32 (2014) 1043–1049. doi:10.1080/10916466.2011.638691.

[8] L.A. Henry, D. Harries, P. Kingston, J.M. Roberts, Historic scale and persistence of drill cuttings impacts on North Sea benthos, Mar. Environ. Res. 129 (2017) 219–228. doi:10.1016/j.marenvres.2017.05.008.

[9] M. Ghazi, G. Quaranta, J. Duplay, R. Hadjamor, M. Khodja, H.A. Amar, Z. Kessaissia, Life-Cycle Impact Assessment of oil drilling mud system in Algerian arid area, Resour. Conserv. Recycl. 55 (2011) 1222–1231. doi:10.1016/j.resconrec.2011.05.016.

[10] Ministry of Environment & Claimt afferias, MD 18-93 Regulations for the Management of Hazardous Waste, (1993).

[11] S.A. Abdul-Wahab, G.A. Al-Rawas, S. Ali, H. Al-Dhamri, Impact of the addition of oil-based mud on carbon dioxide emissions in a cement plant, J. Clean. Prod. 112 (2016) 4214–4225. doi:10.1016/j.jclepro.2015.06.062.

[12] S.J. Cripps, Disposal of oil-based cuttings, 1998.

[13] M.F. Strachan, Studies on the impact of a water-based drilling mud weighting agent (Barite) on some Benthic invertebrates, (2010) 13–17. file:///C:/Users/em0899/Desktop/hilal2017/Journals 2018/OBM/studies on the impact of a water-based drilling mud in North Sea.pdf.

[14] M.F. Fakoya, R.M. Ahmed, A generalized model for apparent viscosity of oil-based muds, J. Pet. Sci. Eng. 165 (2018) 777–785. doi:10.1016/j.petrol.2018.03.029.

[15] O.E. Agwu, A.N. Okon, F.D. Udoh, A Comparative Study of Diesel Oil and Soybean Oil as Oil-Based Drilling Mud, J. Pet. Eng. (2015). doi:10.1155/2015/828451.

[16] M.I. Abduo, A.S. Dahab, H. Abuseda, A.M. AbdulAziz, M.S. Elhossieny, Comparative study of using Water-Based mud containing Multiwall Carbon Nanotubes versus Oil-Based mud in HPHT fields, Egypt. J. Pet. 25 (2016) 459–464. doi:10.1016/j.ejpe.2015.10.008.

[17] D. Lechtenberg, H. Diller, Alternative Fuels and Raw Materials (AFR) review “oil mud drillings,” in:

Altern. Fuels Raw Mater. Handb. Cem. Lime Ind. Vol. 2, MVW Lechtenberg & Partner, Dusseldorf, 2012: pp. 303–320.

[18] Industrail and Hazardous Waste Survey Summery Report. Oman: Oman Environmental Service Holding Company S.A.O.C (be'ah), 2018.

[19] Petroleum Development Oman, http:\\www.pdo.co.om [Accessed on 1 Feb. 2019], www.pdo.om

[20] Dhofar Cement Company, [Accessed on 1 November 2018], http://www.dhofarcement.com/products.htm

[21] Oman cement: Setting up of new company. News Bites - Construction. Aug 16 2016. Available from: http://0-search.proquest.com.wam.leeds.ac.uk/docview/1811542044?accountid=14664. Bites, No Title, (2016).

[22] Sohar Cement Company, [Accessed on 1 November 2018] https://ems.peie.om

[23] Al Madina Cement Company, [Accessed on 1 November 2018], https://amccllc.en.ecplaza.net , Oman.

[24] Oman Cement Company SAOG, [Accessed on 1 Novmber 2018], http:\\www.occ.om

[25] P.A.M. Basheer, S. Barbhuiya, Different types of cement used in concrete, in: ICE Man. Constr. Mater., 2009: pp. 61–68. doi:10.1680/mocm.35973.0061.

[26] Walter H. Duda, Cement-Data-Book: International Process Engineering in the Cement Industry, Bauverlag GmbH, Wiesbaden, 1975.

[27] C.T. Galbenis, S. Tsimas, Use of construction and demolition wastes as raw materials in cement clinker production, China Particuology. 4 (2006) 83–85. doi:10.1016/S1672-2515(07)60241-3.

[28] J. Schoon, K. De Buysser, I. Van Driessche, N. De Belie, Fines extracted from recycled concrete as alternative raw material for Portland cement clinker production, Cem. Concr. Compos. 58 (2015) 70–80. doi:10.1016/j.cemconcomp.2015.01.003.

[29] A. Aranda Usón, A.M. López-Sabirón, G. Ferreira, E. Llera Sastresa, Uses of alternative fuels and raw materials in the cement industry as sustainable waste management options, Renew. Sustain. Energy Rev. 23 (2013) 242–260. doi:10.1016/j.rser.2013.02.024.

[30] M. De Schepper, K. De Buysser, I. Van Driessche, N. De Belie, The regeneration of cement out of Completely Recyclable Concrete: Clinker production evaluation, 2013. doi:10.1561/2200000016.

[31] A. Shahriar, Investigation on Rheology of Oil Well Cement Slurries, 2011. http://ir.lib.uwo.ca/etd.

[32] J.N. de Paula, J.M. Calixto, L.O. Ladeira, P. Ludvig, T.C.C. Souza, J.M. Rocha, A.A.V. de Melo, Mechanical and rheological behavior of oil-well cement slurries produced with clinker containing carbon nanotubes, J. Pet. Sci. Eng. 122 (2014) 274–279. doi:10.1016/j.petrol.2014.07.020.

[33] E. Kuzielová, M. Žemlička, J. Másilko, M.T. Palou, Pore structure development of blended G-oil well cement submitted to hydrothermal curing conditions, Geothermics. 68 (2017) 86–93. doi:10.1016/j.geothermics.2017.03.001.

[34] C. Arbelaez, THE PRODUCTION OF API CLASS H OILWELL CEMENT, (n.d.). file:///C:/Users/em0899/AppData/Local/Mendeley Ltd./Mendeley Desktop/Downloaded/Arbelaez - Unknown - THE PRODUCTION OF API CLASS H OILWELL CEMENT.pdf.

[35] American Petroluem Institute, Specification for Cements and Materials for Well Cementing 10A, (2010).

[36] ISO 10426-1:2009:, Petroleum and natural gas industries - Cements and materials for well cementing - Part 1: Specification, (2009).

[37] American Petroluem Institute, Specification for Quality Management System Requirements for Manufacturing Organization for the Petroleum and Natural Gas Industry, API Spec Q1, (2013).

[38] P. Hewlett, Lea" s Chemistry of Cement and Concrete, 2004. doi:10.1016/B978-0-7506-6256-7.50031-X.

[39] P. Stutzman, A. Heckert, A. Tebbe, S. Leigh, Uncertainty in Bogue-calculated phase composition of hydraulic cements, Cem. Concr. Res. 61–62 (2014) 40–48. doi:10.1016/j.cemconres.2014.03.007.

[40] Y. Shen, J. Qian, Y. Huang, D. Yang, Synthesis of belite sulfoaluminate-ternesite cements with phosphogypsum, Cem. Concr. Compos. 63 (2015) 67–75.

[41] H. Al-Dhamri, K. Melghit, Use of alumina spent catalyst and RFCC wastes from petroleum refinery to substitute bauxite in the preparation of Portland clinker, J. Hazard. Mater. 179 (2010) 852–859. doi:10.1016/j.jhazmat.2010.03.083.

[42] European Standard, EN 196-2, Methods of testing cement-Part 2: Chemical analysis of cement, Determination of loss on ignition., 2005.

[43] ASTM International, Extraction of Free Lime in Portland Cement and Clinker by Ethylene Glycol, in: Rapid Methods Chem. Anal. Hydraul. Cem., 1988. doi:10.1520/STP34297S.

[44] R. Delimi, Determination of Free Lime in Industrial Products, (1991) 593–600.

[45] K. Scrivener, A. Bazzoni, B. Mota, John E. Rossen, Electron Microscopy, in: A Pract. Guid. to Microstruct. Anal. Cem. Mater., Taylor & Francis, 2015: pp. 351–417. doi:10.1021/ac60237a015.

[46] G. Description, Thermogravimetric Analysis, in: A Pract. Guid. to Microstruct. Anal. Cem. Mater., Taylor & Francis, 2015. doi:10.1038/1731011b0.

[47] European Standard, EN 451-1, Methods for Portland Cement Testing, Methods of testing fly ash-Part:1 Determination of free calcium oxide content, 2005.

[48] A. Al-Maqbali, S. Feroz, G. Ram, Hilal Al-Dhamri, Feasibility Study on Spent Pot Lining (SPL) as Raw Material in Cement Manufacture Process, Int. J. Environ. Chem. 2 (2016) 18–26.

[49] Robert E. Carver, Procedures in Sedimentary Petrology, Wiley-Interscience, California, 1971.

[50] H. Donald, E XAMINATION AND I NTERPRETATION OF Microscopical Examination and Interpretation of Portland Cement and Clinker, 2nd Editio, Portland Cement Association, 1999.

[51] ASTM, Petrography of Cementitious Materials: Petrographic Methods for Analysis of Cement Clinker and Concrete Microstructure, USA, 1994. doi:10.1520/STP1215-EB.

[52] P.C. Hewlett, The Constitution and Specification of Cement Clinker.Pdf, in: Lea´s Chem. Cem. Concret (4th Ed., Fourth Edi, Elsevier Ltd., 1998: pp. 131–193. doi:10.1016/B978-0-7506-6256-7.50016-3.

[53] J. Bensted, Special Cements, in: Lea's Chem. Cem. Concr., Fourth Edi, Elsevier Ltd., 2003: pp. 783–840. doi:10.1016/B978-075066256-7/50026-6.

[54] A.M.M. Soltan, W.A. Kahl, M.M. Hazem, M. Wendschuh, R.X. Fischer, Thermal microstructural changes of grain-supported limestones, Mineral. Petrol. 103 (2011) 9–17. doi:10.1007/s00710-011-0151-0.

[55] A.M. Soltan, W.-A. Kahl, M. Wendschuh, M. Hazem, Microstructure and reactivity of calcined mud supported limestones, Miner. Process. Extr. Metall. 121 (2012) 5–11. doi:10.1179/1743285511Y.0000000024.

[56] I. Allegretta, D. Pinto, G. Eramo, Effects of grain size on the reactivity of limestone temper in a

kaolinitic clay, Appl. Clay Sci. 126 (2016) 223–234. doi:10.1016/j.clay.2016.03.020.

[57] A.W.D. Hills, The mechanism of the thermal decomposition of calcium carbonate, Chem. Eng. Sci. 23 (1968) 297–320. doi:10.1016/0009-2509(68)87002-2.

[58] S. Lin, T. Kiga, Y. Wang, K. Nakayama, Energy analysis of CaCO3calcination with CO2capture, Energy Procedia. 4 (2011) 356–361. doi:10.1016/j.egypro.2011.01.062.

[59] J.M. Criado, A. Ortega, A study of the influence of particle size on the thermal decomposition of CaCO3 by means of constant rate thermal analysis, Thermochim. Acta. 195 (1992) 163–167. doi:10.1016/0040-6031(92)80059-6.

[60] D.T. Beruto, R. Botter, R. Cabella, A. Lagazzo, A consecutive decomposition-sintering dilatometer method to study the effect of limestone impurities on lime microstructure and its water reactivity, J. Eur. Ceram. Soc. 30 (2010) 1277–1286. doi:10.1016/j.jeurceramsoc.2009.12.012.

[61] M. Galimberti, N. Marinoni, G. Della Porta, M. Marchi, M. Dapiaggi, Effects of limestone petrography and calcite microstructure on OPC clinker raw meals burnability, Mineral. Petrol. 111 (2017) 793–806. doi:10.1007/s00710-016-0485-8.

[62] N. Marinoni, A. Bernasconi, G. Della Porta, M. Marchi, A. Pavese, The role of petrography on the thermal decomposition and burnability of limestones used in industrial cement clinker, Mineral. Petrol. 109 (2015) 719–731. doi:10.1007/s00710-015-0398-y.

[63] R.J. Dunham, Classification of carbonate rocks according to depositional texture., in: Classif. Carbonate Rocks, Am. Assoc. Pet. Geol. Mem., 1962: pp. 108–121.

[64] A.F. Embry, J.E. Klovan, A Late Devonian reef tract on northeastern Banks Island, NWT, Bull. Can. Pet. Geol. 19 (1971) 730–781. doi:10.5072/PRISM/22817.

[65] S.W. Lokier, M. Al Junaibi, The petrographic description of carbonate facies: are we all speaking the same language?, Sedimentology. 63 (2016) 1843–1885. doi:10.1111/sed.12293.

[66] V.P. Wright, A revised classification of limestones, Sediment. Geol. 76 (1992) 177–185. doi:10.1016/0037-0738(92)90082-3.

[67] P.A. Scholle, D.S. Ulmer-Scholle, A Color Guide to the Petrography of Carbonate Rocks: Grains, Textures, Porosity, Diagenesis, AAPG Memoir, 2003.

[68] N. Marinoni, S. Allevi, M. Marchi, M. Dapiaggi, A kinetic study of thermal decomposition of limestone using in situ high temperature X-ray powder diffraction, J. Am. Ceram. Soc. 95 (2012) 2491–2498. doi:10.1111/j.1551-2916.2012.05207.x.

[69] A. Escardino, J. García-Ten, C. Feliu, A. Moreno, Calcium carbonate thermal decomposition in white-body wall tile during firing. I. Kinetic study, J. Eur. Ceram. Soc. 30 (2010) 1989–2001. doi:10.1016/j.jeurceramsoc.2010.04.014.

[70] A.K. Chatterjee, Chemico-Mineralogical Characteristics of Raw Materials, in: S.N.B.T.-A. in C.T. GHOSH (Ed.), Pergamon, 1983: pp. 39–68. doi:https://doi.org/10.1016/B978-0-08-028670-9.50008-9.

[71] Fredrik P. Glasser, The Burning of Portland Cement, in: P.C. Hewlett (Ed.), Lea's Chem. Cem. Concr., Fourth Edi, Butterworth Heinemann, 1998: pp. 195–240. doi:10.1016/B978-0-7506-6256-7.50017-5.

[72] G. Kakali, K. Kolovos, S. Tsivilis, Incorporation of minor elements in clinker: their effect on the reactivity of the raw mix and the microstructure of clinker, in: 11th Int. Congr. Chem. Cem., Durban, South Africa, 2003: pp. 2885–2897.

[73] W. Kurdowski, Influence of Minor Components on Hydraulic Activity of Portland Cement Clinker, in: Congr. Chem. Cem., Moscow, 1974: pp. 1–4.

[74] K. Kolovos, S. Tsivilis, G. Kakali, The effect of foreign ions on the reactivity of the CaO-SiO2-Al2O3-Fe2O3 system II : Cations, 32 (2001) 463–469.

[75] M.N. De Noirfontaine, S. Tusseau-nenez, M. Signes-frehel, G. Gasecki, C. Girod-labianca, Effect of Phosphorus Impurity on Tricalcium Silicate T 1 : From Synthesis to Structural Characterization, J. Am. Ceram. Soc. 2344 (2009) 1–8. doi:10.1111/j.1551-2916.2009.03092.x.

[76] D. Stephan, R. Mallmann, D. Knöfel, R. Härdtl, High intakes of Cr, Ni, and Zn in clinker Part I. Influence on burning process and formation of phases, Cem. Concr. Res. 29 (1999) 1949–1957. doi:10.1016/S0008-8846(99)00195-7.

[77] D. Stephan, R. Mallmann, D. Knöfel, R. Härdtl, High intakes of Cr, Ni, and Zn in clinker Part II. Influence on the hydration properties, Cem. Concr. Res. 29 (1999) 1959–1967. doi:10.1016/S0008-8846(99)00198-2.

[78] D. Stephan, H. Maleki, D. Knöfel, B. Eber, R. Härdtl, Influence of Cr, Ni, and Zn on the properties of pure clinker phases Part I. C3S, Cem. Concr. Res. 29 (1999) 545–552. doi:10.1016/S0008-8846(99)00009-5.

[79] D. Stephan, H. Maleki, D. Knöfel, B. Eber, R. Härdtl, Influence of Cr , Ni , and Zn on the properties of pure clinker phases Part II . C 3 A and C 4 AF, Cem. Concr. Res. 29 (1999) 651–657. doi:10.1007/s11595-013-0724-3.

[80] K. Kolovos, S. Tsivilis, G. Kakali, SEM examination of clinkers containing foreign elements, Cem. Concr. Compos. 27 (2005) 163–170. doi:10.1016/j.cemconcomp.2004.02.003.

[81] A. Zezulová, T. Staněk, T. Opravil, Influence of barium oxide additions on Portland clinker, Ceram. - Silikaty. 61 (2017) 20–25. doi:10.13168/cs.2016.0055.

[82] X. Guo, S. Wang, L. Lu, H. Wang, Influence of barium oxide on the composition and performance of alite-rich Portland cement, Adv. Cem. Res. 24 (2012) 139–144. doi:10.1680/adcr.10.00033.

[83] N.K. Katyal, S.C. Ahluwalia, R. Parkash, Effect of barium on the formation of tricalcium silicate, Cem. Concr. Res. 29 (1999) 1857–1862. doi:10.1016/S0008-8846(99)00172-6.

[84] J.I. Bhatty, Role of Minor Elements in Cement Manufacture and Use, 1995.

[85] Cohn J., Reactions in solid state, Cem. Rev. 42 (1948) 527.

[86] X. Li, X. Shen, M. Tang, X. Li, Stability of tricalcium silicate and other primary phases in portland cement clinker, Ind. Eng. Chem. Res. 53 (2014) 1954–1964. doi:10.1021/ie4034076.

[87] S. Ma, R. Snellings, X. Li, X. Shen, K.L. Scrivener, Alite-ye'elimite cement: Synthesis and mineralogical analysis, Cem. Concr. Res. 45 (2013) 15–20. doi:10.1016/j.cemconres.2012.10.020.

[88] J. Zhang, C. Gong, S. Wang, L. Lu, X. Cheng, Effect of strontium oxide on the formation mechanism of dicalcium silicate with barium oxide and sulfur trioxide, Adv. Cem. Res. 27 (2015) 381–387. doi:10.1680/adcr.14.00021.

[89] X. Li, W. Xu, S. Wang, M. Tang, X. Shen, Effect of SO3and MgO on Portland cement clinker: Formation of clinker phases and alite polymorphism, Constr. Build. Mater. 58 (2014) 182–192. doi:10.1016/j.conbuildmat.2014.02.029.

[90] N.H. Christensen, F.L. Smidth and Co., Burnability of cement raw mixes at 1400°C II the effect of the fineness, Cem. Concr. Res. 9 (1979) 285–294. doi:10.1016/0008-8846(79)90120-0.

[91] Wieslaw Kurdowski, Portland Cement Clinker, in: Cem. Concr. Chem., Springer, Poland, 2014: pp. 21–123.

[92] F. Dunstetter, M.N. De Noirfontaine, M. Courtial, Polymorphism of tricalcium silicate, the major compound of Portland cement clinker: 1. Structural data: Review and unified analysis, Cem.

Concr. Res. 36 (2006) 39–53. doi:10.1016/j.cemconres.2004.12.003.

[93] M.N. De Noirfontaine, M. Courtial, M. De Noirfontaine, F. Dunstetter, G. Gasecki, M. Signes-Frehel, Tricalcium silicate Ca3SiO5 superstructure analysis: a route towards the structure of the M1 polymorph, Zeitschrift Für Krist. 227 (2012) 102–112. doi:10.1524/zkri.2011.1425.

[94] L. Nicoleau, A. Nonat, D. Perrey, The di- and tricalcium silicate dissolutions, Cem. Concr. Res. 47 (2013) 14–30. doi:10.1016/j.cemconres.2013.01.017.

[95] G. Kakali, Use of secondary mineralizing raw materials in cement production . A case study of a wolframite – stibnite ore, 27 (2005) 155–161. doi:10.1016/j.cemconcomp.2004.02.037.

[96] A. Zapata, P. Bosch, Low temperature preparation of belitic cement clinker, J. Eur. Ceram. Soc. 29 (2009) 1879–1885. doi:10.1016/j.jeurceramsoc.2008.11.004.